AIAA JOURNAL
Vol. 42, No. 4, April 2004

Hypersonic Mixing Enhancement by Compression at a High Convective Mach Number

Bernard Parent* and Jean P. Sislian†
University of Toronto, Downsview, Ontario M3H 5T6, Canada

The effect of an oblique shock and of a Prandtl–Meyer compression fan on the characteristics of the turbulent mixing of a square-cross-section hydrogen jet in hypervelocity air is presented. The air properties before the compression process are set to those found after the first shock of a two-shock external compression shcramjet inlet at a flight Mach number of 11 and an altitude of 34.5 km. The hydrogen properties are such that the convective Mach number is 1.2, the global equivalence ratio is 0.68, and the pressure of the hydrogen matches the pressure of the air at injection. Also presented is an algebraic expression approximating increase in mixing efficiency growth through compression. The algebraic expression is based on available empirical correlations for the turbulent mixing layer and is simplified for the special case of a high-convective-Mach-number mixing layer in which the Mach numbers of both streams are high. The numerical results are obtained by using the WARP code to solve the Favre-averaged Navier–Stokes equations closed by the Wilcox $k\omega$ turbulence model and the Wilcox dilatational dissipation correction, discretized by the Yee–Roe flux-limited scheme. Results obtained indicate increase in the mixing efficiency growth by 5.7 and 6.3 times through the oblique shock and the compression fan, respectively. Despite generating weaker axial vortices, the compression fan results into a greater increase mixing efficiency growth because of a higher density increase.

Nomenclature

c	=	species mass fraction
h	=	height of the free-jet injector
k	=	turbulence kinetic energy
k_{div}	=	user-defined constant used in conjunction with the $k\omega$ model in WARP
l_{int}	=	fuel/air interface length in the cross-stream plane
M	=	Mach number
M_c	=	convective Mach number, $(q_1 - q_2)/(a_1 + a_2)$
$\dot{m}_{\text{O}_2,\text{engine}}$	=	mass flow rate of oxygen in the engine
P	=	pressure
q	=	magnitude of the velocity vector
r	=	mesh dimensions factor
s	=	cross-stream coordinate of the mixing layer
T	=	temperature
u	=	velocity component along x
$\boldsymbol{v}$	=	velocity vector
x, y, z	=	Cartesian coordinates
y^+	=	nondimensional wall distance, $y/\mu\sqrt{(\rho\tau_{\text{w}})}$
δ_m	=	height of the mixing layer
η_m	=	mixing efficiency
ξ_{verge}	=	user-defined convergence criterion threshold
ρ	=	density
φ_{verge}	=	user-defined streamwise ellipticity sensor threshold
$\boldsymbol{\omega}$	=	vorticity vector
$\boldsymbol{\nabla}$	=	gradient vector

Received 17 August 2002; revision received 9 February 2003; accepted for publication 10 June 2003.

*Graduate Student, Institute for Aerospace Studies; bernard.parent@utoronto.ca; currently Research Associate, Department of Aerospace Engineering, Seoul National University, Seoul 151-744, Republic of Korea; bernard@snu.ac.kr. Student Member AIAA.

†Professor, Institute for Aerospace Studies; sislian@caius.utias.utoronto.ca. Associate Fellow AIAA.

Introduction

HYPERSONIC airbreathing flight vehicles, such as the supersonic combustion ramjet (scramjet) or the shock-induced combustion ramjet (shcramjet),[1,2] are generally characterized by extremely small flow residence time in the engine, a consequence of the very high speed of the flight vehicle coupled with the need to avoid significant flow deceleration.[3] This short residence time of the flow particularly handicaps the fuel/air mixing process, which needs to be enhanced significantly if the fuel is to be mixed homogeneously with the incoming air. One promising mixing enhancement strategy at hypervelocities is the so-called shock-enhanced mixing mechanism, in which the interaction between the mixing layer and the oblique shock creates strong axial vortices that stretch the fuel/air interface.[4–7]

The interaction of a mixing layer composed of two streams of different densities with an oblique shockwave induces a misalignment between the density gradient in the mixing layer and the pressure gradient of the shockwave. A misalignment between pressure and density gradients can generate vorticity through the baroclinic torque term of the Helmholtz vorticity transport equation

$$\frac{\partial}{\partial t}\boldsymbol{\omega} + (\boldsymbol{v}\cdot\boldsymbol{\nabla})\boldsymbol{\omega} = \underbrace{\frac{1}{\rho^2}\,\boldsymbol{\nabla}\rho\times\boldsymbol{\nabla}P}_{\text{baroclinic torque}} + \cdots \tag{1}$$

with $\boldsymbol{\omega}$ the vorticity, $\boldsymbol{v}$ the velocity, ρ the density, and P the pressure. A rise in vorticity can be particularly helpful to the mixing process by stretching the mixing-layer interface,[8] hence increasing the mixing. Waitz et al.[4,9–12] and later Lee et al.[6,13] attribute the good performance of ramp injectors partly to the vorticity generated by the baroclinic torque created through shock/mixing layer interactions. In Ref. 7, the baroclinic torque is also considered to be the main driving mechanism of mixing enhancement through interaction of a free jet with an oblique shock. Interestingly, a different explanation for mixing enhancement through an oblique shock is given by Vasilev et al.[5] They find, through a numerical investigation based on the parabolized Navier–Stokes equations, that the convergence in space of the jet (due to the compression of the flow by the oblique shockwave), coupled with the observed negligible changes in the characteristics of turbulence through the shock, results in an increase in mixing by 2 to 4 times. The characteristics of turbulence are also found experimentally by Shau and Dolling[14] not to be

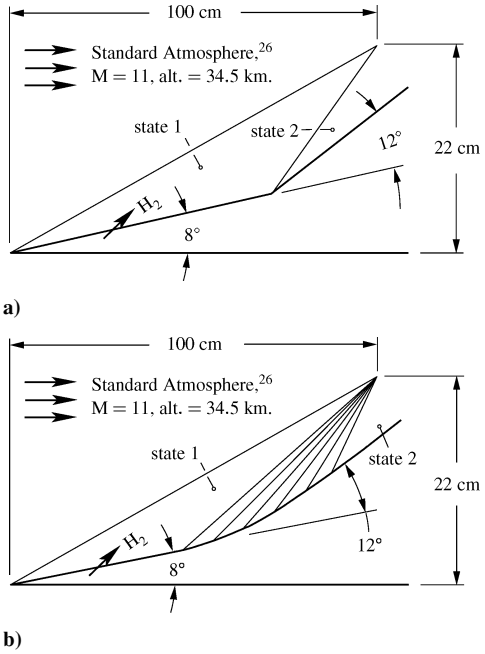

Fig. 1 Schematic of the external compression shcramjet inlet with an a) shock/shock configuration and with a b) shock/compression-fan configuration.

influenced significantly by an oblique shock in the freestream Mach number range 3–5.

While the effect of an oblique shock on the mixing layer has been investigated in several papers, no study has yet been reported on the effect of a Prandtl–Meyer compression fan on the characteristics of the mixing layer. The effect of a Prandtl–Meyer fan is of particular importance when fuel is injected into the inlet of high-speed flight vehicles, where Prandtl–Meyer compression fans are preferred to oblique shocks as a means of reducing losses.

The main objective of this paper is to present a comparison of the effect of an oblique shock and a Prandtl–Meyer compression fan on the characteristics of the turbulent mixing of a square-cross-section hydrogen jet with air at a high convective Mach number. The rise in mixing efficiency is quantified for a shock strength and a compression fan strength typical of those found in an external compression shcramjet inlet at a flight Mach number of 11, as depicted in Fig. 1. The air properties before the compression process are set to those found after the first shock in a two-shock external compression shcramjet inlet at a flight Mach number of 11 and an altitude of 34.5 km. The fuel properties are such that the convective Mach number is 1.2, the global equivalence ratio is 0.68, and the pressure of the hydrogen matches the pressure of the air at injection.

A second objective of this paper is to present an approximate algebraic expression aimed at predicting the mixing efficiency growth through a compression process (either an oblique shock or a compression fan). This mixing efficiency growth equation is based on the available empirical correlations for the turbulent shear layer growth and takes advantage of the properties of the turbulent shear layer when the Mach numbers of both streams are high and when the convective Mach number is high. The mixing efficiency growth equation is then validated through comparisons with numerical data and is used to correlate the mixing efficiency growth increase obtained numerically for a free jet interacting with a compression fan or an oblique shock.

The numerical results are obtained using the Window-Allocatable Resolver for Propulsion (WARP) code,[15,16] in which the multispecies Favre-averaged Navier–Stokes (FANS) equations closed by the Wilcox $k\omega$ turbulence model[17] are discretized by the Yee–Roe flux-limited method.[18] To account for the compressibility effects occurring at a high turbulent Mach number,[16] the Wilcox dilatational dissipation correction[19] is used in conjunction with the $k\omega$ turbulence model. Convergence to steady state is achieved using the marching window acceleration technique.[15] The use of the marching window decreases the work by more than 30 times and the memory required by 5 times for the cases shown herein and permits the solution of significantly finer meshes, hence resulting in decreased numerical error.

Mixing Efficiency Growth Equation

The free turbulent mixing layer can be taken as self-similar[20] and hence as resulting in identical species mass fraction profiles at any x-station in the coordinate system $x - s$, with x the streamwise coordinate and s a cross-stream coordinate defined so that the mixing layer edges are located at $s = 0$ and $s = 1$ for any x-station (Fig. 2). Because the reacting mass fraction of oxygen $c^R_{O_2}$ is solely a function of c_{O_2} and c_{H_2}, and because the profiles of the mass fraction c_{O_2} and c_{H_2} are self-similar in the mixing layer, it follows that the profile of $c^R_{O_2}$ is also self-similar. Mixing efficiency is here defined as the ratio of the mass flux of oxygen that would react if the mixture were ignited to the mass flux of oxygen flowing in the engine, with the latter a constant. Therefore, it follows that for a self-similar mixing layer, as shown in Fig. 2, the mixing efficiency is proportional to

$$\eta_m \sim l_{\text{int}}\delta_m \int_0^1 \rho q c^R_{O_2}\,\mathrm{d}s \tag{2}$$

where $c^R_{O_2}$ is the potential reacting mass fraction of oxygen, δ_m the height of the mixing layer at the x-station under consideration, and l_{int} the fuel/air interface length. It is noted that l_{int} does not need to be introduced to describe the mixing efficiency of the planar mixing layer shown in Fig. 2. Equation (2) is, however, intended to describe the mixing efficiency occurring in a three-dimensional environment where the mixing layer is not necessarily planar. Hence, the mixing efficiency in a three-dimensional environment is here approximated as the product of the interface length l_{int} and the mixing efficiency of a planar mixing layer. As shall be seen subsequently, this is a fairly good approximation for the problems shown herein, especially in the near field, where the mixing layer height δ_m is small compared to the interface length.

Interestingly, for self-similar velocity and density profiles in the mixing layer, the integral on the right-hand side (RHS) of Eq. (2) does not depend on x, and the mixing efficiency is hence only a function of $l_{\text{int}}\delta_m$. However, should the mixing layer traverse a shock or a compression fan, the density of the air and hydrogen streams will increase, and the integral in Eq. (2) will not be constant along x. Nonetheless, if the density is normalized with the density of the air stream, Eq. (2) can be written as

$$\eta_m \sim l_{\text{int}}\delta_m \rho_{\text{air}} \int_0^1 \frac{\rho}{\rho_{\text{air}}} q c^R_{O_2}\,\mathrm{d}s \tag{3}$$

Now, if we assume that 1) the speed of the air and hydrogen streams is not altered by the compression process (which is a fair approximation for the flow in a hypersonic airbreathing engine[3]), and 2) the density ratio increase through the compression process is the same for the hydrogen and air streams, it then follows that the integral on the RHS of Eq. (3) will remain constant as the mixing layer is compressed by a shockwave or a compression fan. The assumption that the fuel and the air exhibit the same density ratio increase through the compression process is an excellent one at hypersonic speeds, as will be shown subsequently through our numerical simulations. From these two assumptions, it follows that

$$\eta_m \sim l_{\text{int}}\delta_m \rho_{\text{air}} \tag{4}$$

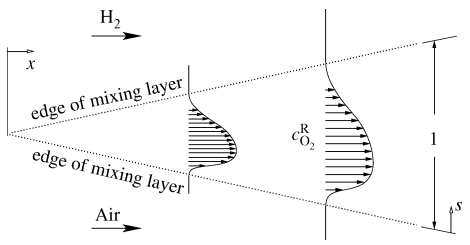

Fig. 2 Schematic of a turbulent mixing layer with the reacting mass fraction of oxygen $c^R_{O_2}$ being self-similar.

Well upstream or downstream of the compression process, where the air density and interface length do not vary significantly with respect to x, the mixing efficiency growth can be written as

$$\frac{\mathrm{d}}{\mathrm{d}x}\eta_m \sim l_{\mathrm{int}}\rho_{\mathrm{air}}\frac{\mathrm{d}}{\mathrm{d}x}\delta_m \tag{5}$$

It is emphasized that the latter is not valid through the compression process and can only be applied to the flow regions in which no compression is occurring. Replacing the last term on the RHS of Eq. (5) with the empirical correlation proposed by Brown and Roshko[21,22] multiplied by the compressibility correction factor for compressible shear layers outlined by Papamoschou and Roshko,[23] we get

$$\frac{\mathrm{d}}{\mathrm{d}x}\eta_m \sim l_{\mathrm{int}}\rho_{\mathrm{air}} \times \underbrace{(q_{\mathrm{H_2}} - q_{\mathrm{air}})}_{\substack{\text{speed difference}\\ \text{between the two}\\ \text{streams}}} \times \underbrace{\frac{\sqrt{\rho_{\mathrm{H_2}}} + \sqrt{\rho_{\mathrm{air}}}}{q_{\mathrm{H_2}}\sqrt{\rho_{\mathrm{H_2}}} + q_{\mathrm{air}}\sqrt{\rho_{\mathrm{air}}}}}_{\substack{\text{reciprocal of the}\\ \text{incompressible average}\\ \text{vortex speed}}}$$

$$\times \underbrace{f_\rho}_{\substack{\text{Brown–Roshko}\\ \text{correction for}\\ \text{density difference}}} \times \underbrace{f(M_c)}_{\substack{\text{Papamoschou–}\\ \text{Roshko correction}\\ \text{for compressible}\\ \text{shear layer}}} \tag{6}$$

where the Papamoschou–Roshko correction for compressible shear layers can be found in Refs. 20 and 23 to correspond to $f(M_c) = 0.2 + 0.8\exp(-3M_c^2)$, and where q_{air} and $q_{\mathrm{H_2}}$ refer to the speed of the air stream and the speed of the hydrogen stream, respectively. Recall that the convective Mach number M_c can be taken as $(q_{\mathrm{H_2}} - q_{\mathrm{air}})/(a_{\mathrm{H_2}} + a_{\mathrm{air}})$. In Eq. (6), it is noted that neither the speed difference between the two streams nor the incompressible average vortex speed is altered by compression if the speed of each stream is not altered and if the density ratio increase for each stream is the same. Because these two assumptions have already been made, Eq. (6) can be recast to

$$\frac{\mathrm{d}}{\mathrm{d}x}\eta_m \sim l_{\mathrm{int}}\rho_{\mathrm{air}} f_\rho f(M_c) \tag{7}$$

Furthermore, there is a weak dependence of the mixing layer growth on the Brown–Roshko density difference correction, the latter varying by less than 5% (see Fig. 1 in Dimotakis[20]) in the range $\frac{1}{7} < \rho_2/\rho_1 < 7$. This justifies our third, and last, assumption to neglect the effect of density difference on the mixing efficiency growth:

$$\frac{\mathrm{d}}{\mathrm{d}x}\eta_m \sim l_{\mathrm{int}}\rho_{\mathrm{air}} f(M_c) \tag{8}$$

It can hence be seen that the growth of the mixing efficiency is a function primarily of the air density, the convective Mach number, and the fuel/air interface length. A compression process increases the density and decreases the convective Mach number, hence contributing to an increase in the mixing efficiency growth. However, a compression process also converges the fuel jet cross-section, which results in a decrease in the interface length and hence contributes to a decrease of the mixing efficiency growth. The interface length can also be stretched by the axial vortices created by the interaction between the compression wave and the mixing layer. Some numerical experiments are now performed to validate Eq. (8) and to assess quantitatively, with the help of Eq. (8), the separate gains and losses in mixing efficiency growth through an oblique shock and a compression fan by 1) density increase, 2) convective Mach number decrease, 3) decrease in interface by jet cross-sectional area compression, and 4) interface stretching by axial vortices.

Problem Setup

Three configurations are considered: 1) a freejet over a flat plate as in Fig. 3a, 2) a freejet intersecting an oblique shockwave as in Fig. 3b, and 3) a freejet intersecting a compression fan as shown in Fig. 3c. The test cases outlined in Table 1 are referred to by strings composed of a letter related to the geometry of the problem followed by a number related to the inflow conditions. The letter "N" refers to a free jet over a flat plate and the letter "S" refers to a free jet over a 12-deg wedge, whereas the letter "F" refers to a free jet over a Prandtl–Meyer compression surface with a total flow turning angle of 12 deg. The mixing region length is set to 80 cm in all cases and the injector array spacing is set to 6 cm. The position of the shock from the start of the mixing layer is found from an on-design external compression inlet of length 1 m with the fuel injected 35 cm downstream from the inlet leading edge. In all cases,

Table 1 Test cases

Case	Configuration	Air and H_2 inflow	h, cm	f, M_c	ρ_{air}, kg/m^3	l_{int}, cm
N1	Flat plate	State 1[a]	2.0	0.211	0.036	4.0
N2	Flat plate	State 2[b]	0.65	0.289	0.111	2.65
N3	Flat plate	ρ, q from state 1, T from state 2[c]	2.0	0.289	0.036	4.0
S1	Oblique shock	State 1	2.0	0.211	0.036	4.0
F1	Compression fan	State 1	2.0	0.211	0.036	4.0

[a]In state 1, the air properties correspond to $P = 4758$ Pa, $T = 462$ K, $q = 3328$ m/s and the hydrogen properties correspond to $P = 4758$ Pa, $T = 243$ K, $q = 5257$ m/s.
[b]In state 2, the air properties correspond to $P = 28{,}500$ Pa, $T = 900$ K, $q = 3328$ m/s, and the hydrogen properties correspond to $P = 28{,}500$ Pa, $T = 473$ K, $q = 5257$ m/s.
[c]The resulting pressure is 9266 Pa.

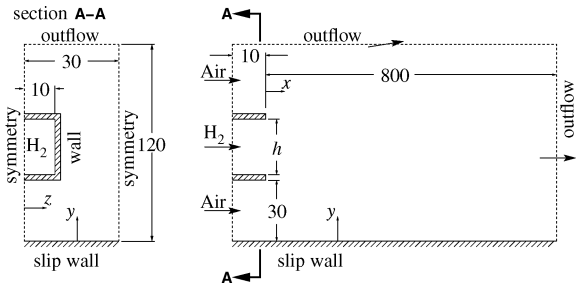

a) Flat plate configuration

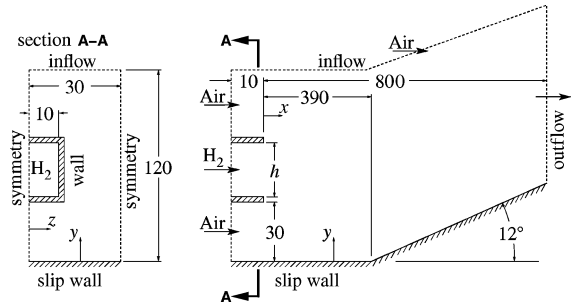

b) Oblique shock configuration

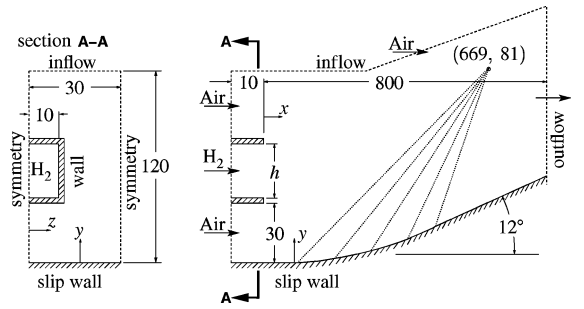

c) Compression fan configuration

Fig. 3 Schematic of the computational domain and boundary conditions for the a) flat plate, b) oblique shock, and c) Prandtl–Meyer compression fan configurations; all dimensions in millimeters.

the bottom boundary is set to a slip wall, to avoid a boundary-layer effect on the mixing layer properties. On no-slip wall surfaces, the temperature is fixed to the temperature of the incoming air.

For cases N1, F1, and S1, the air and fuel inflow conditions are fixed to those in state 1. The air properties in state 1 correspond to the flow conditions downstream of the first shock of the shcramjet inlet depicted in Fig. 1 at a flight Mach number of 11 and an altitude of 34.5 km (the altitude being a consequence of a flight dynamic pressure fixed to 67,032 Pa). The hydrogen properties in state 1 are such that the convective Mach number is 1.2, the global equivalence ratio is 0.68, and the pressure of the hydrogen matches the pressure of the air. The resulting hydrogen pressure, temperature, and speed in state 1 are 4758 Pa, 243 K, and 5257 m/s, and the air pressure, temperature, and speed correspond to 4758 Pa, 462 K, and 3328 m/s. The global equivalence ratio is calculated assuming a shcramjet inlet height of 0.22 m, for which the oxygen mass flow rate per unit depth is 2.04 kg/ms. To validate the mixing efficiency growth equation for simultaneous changes in flow density, fuel–air interface length, and convective Mach number, we consider case N2, in which the inflow conditions are set to state 2 (see Fig. 1) with the height of the fuel jet reduced so that the global equivalence ratio remains 0.68. In state 2, the speeds of the hydrogen and air streams correspond to those in state 1, while the pressure and temperature correspond to 28,500 Pa and 900 K for the air stream and to 28,500 Pa and 473 K for the hydrogen stream. Finally, for case N3, the inflow density and speed are taken from state 1, while the inflow temperature is taken from state 2. Coincidentally, this results in nearly identical fuel and air inflow pressure. A comparison between cases N1 and N3 can hence reveal the sole effect of the convective Mach number decrease, since only the temperature is altered, keeping constant the density and the interface length.

Numerical Considerations

Unless otherwise indicated, the mesh size is fixed to $385 \times 251 \times 61$ nodes, resulting in similar grid-induced error for all cases. The grid of case F1 is shown in Fig. 4. It is noted that 84% of the gridlines in the streamwise direction are allocated to the mixing layer region, with the rest allocated to the 1-cm-long flat plate prior to the start of the mixing layer. A wall node spacing of 30 μm is used at all no-slip wall surfaces, which results in a value of y^+ at the wall of approximately 2 for the incoming air and of approximately 1.5 for the hydrogen. A value for k_{div} of 10^3 m^2/s^2 is used for all cases and is verified to be below the recommended value of $\frac{1}{10}$ of the maximum value of the turbulence kinetic energy in the boundary layer.[15] (The maximum value for k reaches 2×10^5 m^2/s^2 in the hydrogen boundary layer and 3×10^4 m^2/s^2 in the air boundary layer at $x = 0$ m.) Proper resolution of the air and hydrogen boundary layer prior to injection is not critical for accurate prediction of mixing efficiency for the cases in this paper due to the minimal influence of incoming turbulence on the growth of the mixing layer at a high convective Mach number. A grid convergence study of the mixing efficiency

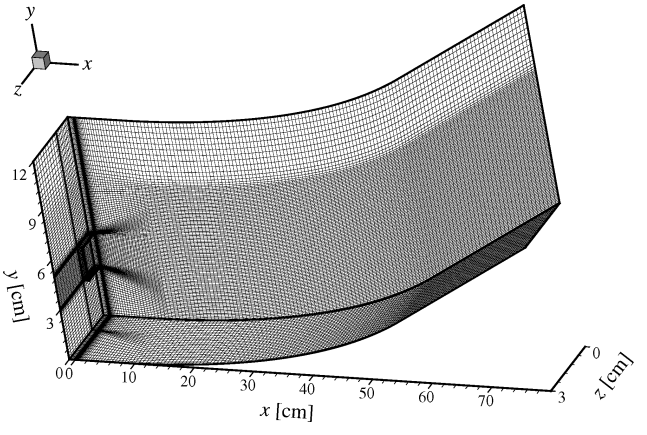

Fig. 4 Mesh used for case F1 with a grid dimensions factor $r = 0.44$ (resulting in $172 \times 112 \times 27$ nodes).

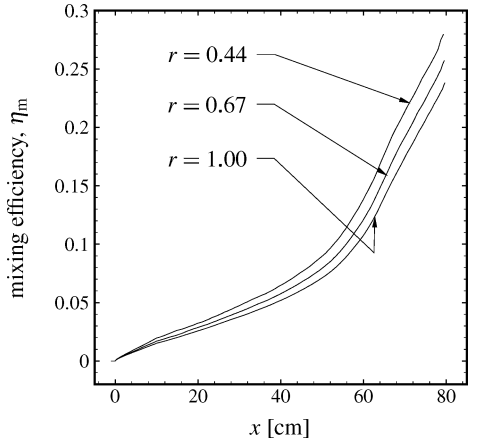

Fig. 5 Grid convergence study of the mixing efficiency of case F1; at $r = 0.44$, $r = 0.67$, and $r = 1.00$, the mesh is composed of $172 \times 112 \times 27$ nodes, $257 \times 167 \times 41$ nodes, and $385 \times 251 \times 61$ nodes, respectively.

over three different mesh levels at grid dimensions factors $r = 0.44$, $r = 0.65$, and $r = 1.0$ is shown in Fig. 5 for case F1. It is noted that the number of gridlines along each mesh dimension is proportional to the "grid dimensions factor" r. Through comparisons with grid convergence studies of planar mixing layers, the relative error in the mixing efficiency for the $385 \times 251 \times 61$ mesh (i.e., $r = 1.0$) is estimated to be 10–15% for case F1. The convergence threshold, ξ_{verge}, is fixed to 4×10^2 s^{-1}, this has been shown[16] to be adequate for a similar problem. In conjunction with the marching window acceleration technique, the streamwise ellipticity sensor threshold φ_{verge} is set to 7×10^4 s^{-1}, resulting in typically 60–80 effective iterations to attain convergence. Last, the turbulent Prandtl number and the turbulent Schmidt number are set to 0.9 and 1.0, respectively.

Mixing Efficiency

The air-based mixing efficiency η_m at the station of interest (here denoted by the subscript b) is defined as the ratio of the mass flux of oxygen that would react should the mixture be ignited to the mass flux of oxygen entering a 0.22-m-high Mach 11 shcramjet inlet at an altitude of 34.5 km:

$$\eta_m \equiv \int_b c^R_{\text{O}_2} \, \text{d}\dot{m} \Big/ \dot{m}_{\text{O}_2,\text{engine}} \tag{9}$$

with $\dot{m}_{\text{O}_2,\text{engine}}$ corresponding to 0.0612 kg/s. The mass fraction of reacting oxygen $c^R_{\text{O}_2}$ corresponds to

$$c^R_{\text{O}_2} = \min\left(c_{\text{O}_2}, c^S_{\text{O}_2} c_{\text{H}_2} \Big/ c^S_{\text{H}_2}\right) \tag{10}$$

with the stoichiometric mass fraction of hydrogen $c^S_{\text{H}_2}$ corresponding to 0.02876 and the stoichiometric mass fraction of oxygen $c^S_{\text{O}_2}$ equal to 0.22824.

Results and Discussion

Validation of the Mixing Efficiency Growth Equation

The validity of Eq. (8) for predicting the effect of a change in the convective Mach number is assessed by comparing the mixing efficiency growth of cases N1 and N3. Recall that in case N1, the fuel and air inflow properties are set to the low-pressure–temperature state 1. In case N3, the air and fuel inflow density and speed are set to the low-pressure–temperature state 1, and the temperature is set to the high-pressure–temperature state 2. A comparison of the mixing efficiency growth between the two cases hence reveals the sole effect of a change in convective Mach number, by avoiding the effects of a change in density and to a large extent of a change in the fuel/air interface length. The decrease in convective Mach number between the two cases translates into a 37% increase of the Papamoschou–Roshko correction term, as shown in Table 1. Because the initial interface length and the air density are equal for the two cases, the

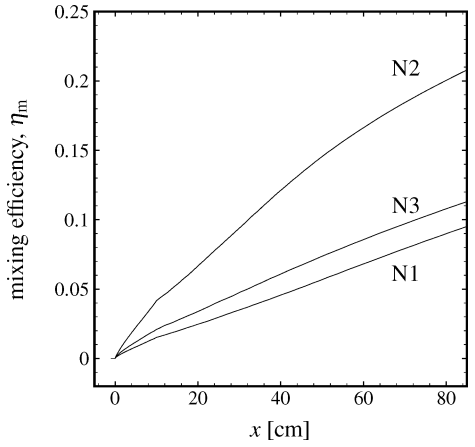

Fig. 6 Mixing efficiency of the flat plate configurations N1, N2, and N3.

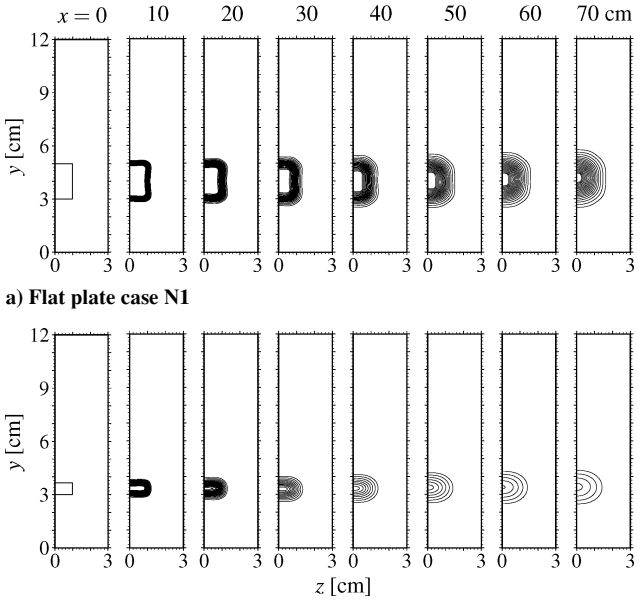

a) Flat plate case N1

b) Flat plate case N2

Fig. 7 Comparison of the hydrogen mass fraction contours between cases a) N1 and b) N2; the contours of the mass fraction of hydrogen are fixed to $c_{H_2} = 0.05, 0.10, \ldots, 0.90, 0.95$.

postulated Eq. (8) hence predicts the mixing efficiency growth of case N3 to be 1.37 times the growth of case N1. On the other hand, as shown in Fig. 6, the ratio of the numerically obtained mixing efficiency growth in cases N3 and N1 is 1.24, or 9% less than the ratio predicted by Eq. (8). This error is attributed to a discrepancy in the shear layer growth predicted by the Papamoschou–Roshko empirical correction and the growth predicted by the $k\omega$ turbulence model (including the Wilcox dilatational dissipation correction) in the convective Mach number range $0.8 \leq M_c \leq 1.2$. This discrepancy was observed[24,25] in a separate study of planar compressible shear layers, where the decrease in shear layer growth was seen to be more pronounced for the empirical correlation than for the $k\omega$ turbulence model, in the convective Mach number range $0.8 \leq M_c \leq 1.2$. The discrepancy between the mixing efficiency growth equation and the numerical results could also be a consequence of a possible small difference in interface length between cases N1 and N3 in the far field. Although the fuel/air interface length of case N1 matches the interface length of case N3 at the point of injection, the interface length does not remain constant throughout the mixing region because of the spreading of the interface by turbulence. However, this effect is seen to play a secondary role in this case, considering that the difference in mixing efficiency growth between cases N1 and N3 in the far field ($20 \leq x \leq 60$ cm) does not vary significantly from the difference in mixing efficiency growth at the point of injection, where the interface length is identical for the two cases (Fig. 6). Farther downstream, for $x > 60$ cm, the difference in mixing efficiency growth between cases N1 and N3 is seen to be attenuated greatly. As shall be seen shortly, this attenuation in mixing in the far field is a consequence of the shear loss occurring at the center of the fuel jet and is not believed to be related to a change in effective interface length due to further interface spreading.

To assess the validity of Eq. (8) under simultaneous changes in density, initial interface length, and convective Mach number, we now compare the mixing efficiency growth of the flat plate configuration N1 (where the air and fuel inflow conditions are taken from the low-pressure–temperature state 1) with the mixing efficiency growth of the flat plate configuration N2 (where the air and fuel inflow conditions are taken from the high-pressure–temperature state 2). For both cases, assuming that the interface spreading by turbulence affects negligibly the interface length, the fuel/air interface length can be taken as constant along the streamwise coordinate, since the pressure of the fuel matches the pressure of the air at injection, preventing compression or expansion of the fuel jet (Fig. 7). By comparing the inflow conditions of case N2 to case N1 in Table 1, it can be seen that the air density is 3.08 times higher, the fuel/air interface length is 1.51 times smaller, and the Papamoschou–Roshko correction term is 1.37 times higher. Therefore, Eq. (8) predicts a mixing efficiency growth ratio between cases N2 and N1 of 2.79. This prediction agrees remarkably well with the mixing efficiency growth ratio of 2.47 observed numerically, as shown in Fig. 6. The 11% overprediction by Eq. (8) is attributed again to the slight discrepancy between the $k\omega$ turbulence model used herein and the Papamoschou–Roshko correction term in the convective Mach number range $0.8 \leq M_c \leq 1.2$. It is emphasized that the inflow speeds of both the air and the fuel streams are not altered between cases N1 and N2. This effectively guarantees that the 11% overprediction of Eq. (8) in this case is not due to the assumptions of constant speed involved in its derivation. Therefore, the difference between the numerical results and Eq. (8) is here attributed solely to differences between the turbulence model and the empirically based mixing-layer growth correlation.

Note that the numerically determined mixing efficiency growth is taken as the average value of the growth in the range $0.2 \leq x \leq 0.5$ m for cases N1, N2, and N3. In this way, the near-field effect of the incoming boundary layer and the far field effect of the lack of a sustained shear are minimized.

Mixing Enhancement by Oblique Shock

The mixing efficiency growth equation was shown in the previous subsection to be accurate within 11% error when compared to numerical results for known variations in air density, convective Mach number, and fuel–air interface. For the shock–mixing layer interaction present in case S1, Eq. (8) cannot be used to predict entirely the mixing efficiency growth increase through the shock, since the stretch in fuel/air interface by the axial vortices generated by the compression process cannot be predicted a priori. Nonetheless, if we can somehow predict the air density increase, the convective Mach number decrease, and the interface decrease due to jet compression, and assuming that the only other physical phenomenon that can influence the mixing efficiency growth is the interface stretching by axial vortices, it follows that the difference between the mixing efficiency growth obtained numerically and the growth given by Eq. (8) is the effect of interface stretching by axial vortices. The purpose of this subsection is hence to compare the change in mixing efficiency growth through the oblique shock of case S1 as estimated by Eq. (8) to the change obtained numerically and to isolate the sole effect of interface stretching due to axial vortices.

The main difficulty lies in predicting the air and fuel properties after the shock, more specifically the density, the temperature, and the fuel jet cross-sectional area. The approach here taken is to assume that the air is compressed by the 12-deg wedge just as if the fuel were not present. This is a fairly good assumption in the case of hydrogen mixed in near-stoichiometric proportions with an incoming

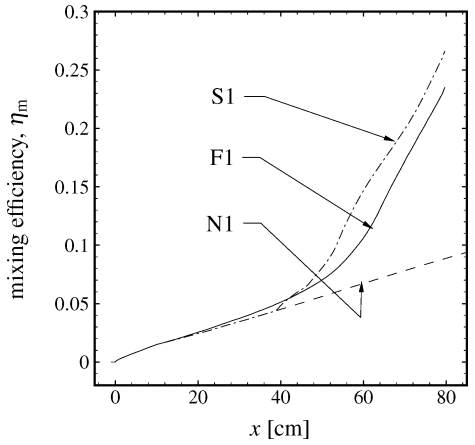

Fig. 8 Comparison of the mixing efficiency between cases N1 (free jet over a flat plate), S1 (free jet traversing an oblique shock), and F1 (free jet traversing a compression fan).

hypersonic stream of air since the total energy, momentum, and mass flow rate of the incoming air are significantly greater than those of the injected fuel. Using the one-dimensional Rankine–Hugoniot equations and assuming a specific heat ratio of $\frac{7}{5}$, we can obtain the air density, pressure, temperature, and speed after the oblique shock. In this manner, an air density ratio of 3.17 is found. Then, again using the Rankine–Hugoniot equations with a specific heat ratio of $\frac{7}{5}$, a flow turning angle for the fuel such that the pressure ratio across the oblique shock is the same as the air pressure ratio previously found is iteratively determined. This results in a fuel turning angle of 21.1 deg, from which the hydrogen temperature and speed after the shock can be obtained. Given the fuel and air speed and temperature before and after the shock, the convective Mach number before and after the compression can be calculated, from which we obtain a Papamoschou–Roshko term ratio across the compression process of 1.56. Also, given the mass flow rate, speed, and density of the hydrogen stream after the shock, the hydrogen cross-sectional area can be determined. From the hydrogen cross-sectional area, the fuel/air interface length after the shock can be found to correspond to 0.62 times the interface length prior to the shock, assuming that the jet is compressed only along the y coordinate.

Therefore, the mixing efficiency growth after the oblique shock is estimated by Eq. (8) to be 3.05 times the mixing efficiency growth before the shock. Shown in Fig. 8, the mixing efficiency growth obtained numerically after the shock is observed to be 5.7 times that obtained before the shock. This leads to the conclusion that the axial vortices alone are responsible through fuel/air interface stretching for a considerable 1.87 times increase in the mixing efficiency growth for the oblique shock configuration. This is confirmed by the visible stretching of the hydrogen mass fraction contours in Fig. 9a. Note that the mixing efficiency growth after the shock is taken as the average mixing efficiency growth in the range $52 \leq x \leq 72$ cm.

Mixing Enhancement by Compression Fan

The process of the determination of the interface stretching by axial vortices outlined in the previous subsection is repeated here for the Prandtl–Meyer compression process of case F1. Assuming that the air is compressed isentropically along the ramp just as if the fuel were not present, the air density after the compression process is found to correspond to 4.07 times the air density at the inflow. To estimate the fuel jet properties, it is assumed that the fuel is also compressed isentropically and that the fuel and air pressure at the end of the compression fan are equal. This results in a Papamoschou–Roshko correction term after the fan of 1.33 times its value prior to the fan, as outlined in Table 2. Further, assuming as in the preceding subsection that the fuel jet is compressed along the y coordinate only, the fuel/air interface length after the fan is predicted to be 0.64 times the interface length prior to the fan.

From these predicted changes in air density, Papamoschou–Roshko correction term, and interface length, the mixing efficiency growth after the fan is therefore predicted by Eq. (8) to be 3.46 times the mixing efficiency growth before the fan. As shown in Fig. 8, the mixing efficiency obtained numerically reveals a growth after the fan that is 6.26 times the growth before the fan, leading to the conclusion that the axial vortices alone contribute to a rise in the mixing efficiency growth by 1.81 times in this case. The numerically obtained mixing efficiency growth is here taken after the fan in the range $62 \leq x \leq 80$ cm.

It is noted that shortly after the compression, the hydrogen jet is eroded by the mixing process, resulting in a sudden loss of shear in the center of the fuel jet. However, this loss in shear does not immediately alter the mixing efficiency growth; significant changes in the latter become apparent much farther downstream from the point of shear loss. This is because the mixing efficiency growth of a hydrogen–air mixing layer is mostly a function of the spread of the mixing layer in the air-dominated region, while being mostly independent of the spread in the hydrogen-dominated region. A sudden loss of shear in the hydrogen-dominated region is hence expected not to translate into a significant decrease in mixing efficiency growth until the decrease in shear reaches the air-dominated region. This is observed numerically for the flat plate case N2: the loss in shear at the center of the fuel jet is seen to occur at $x = 25$ cm, whereas the mixing efficiency growth starts to decrease farther downstream at $x = 65$ cm. This provides a possible explanation for the quasi-constant mixing efficiency growth in the range $50 \leq x \leq 80$ cm for case F1 (Fig. 8) despite the evident loss in shear at the center of the fuel jet at $x = 50$ cm.

Table 2 Predicted and numerically determined mixing efficiency growth ratio through a compression fan and an oblique shock

Effect	Shock S1	Fan F1
Predicted ratio in air density	3.17	4.07
Predicted ratio in the Papamoschou–Roshko correction term	1.56	1.33
Predicted ratio in interface length due to jet compression	0.62	0.64
Numerically obtained ratio in mixing efficiency growth	5.70	6.26
Deduced ratio in interface length due to axial vortices	1.87	1.81

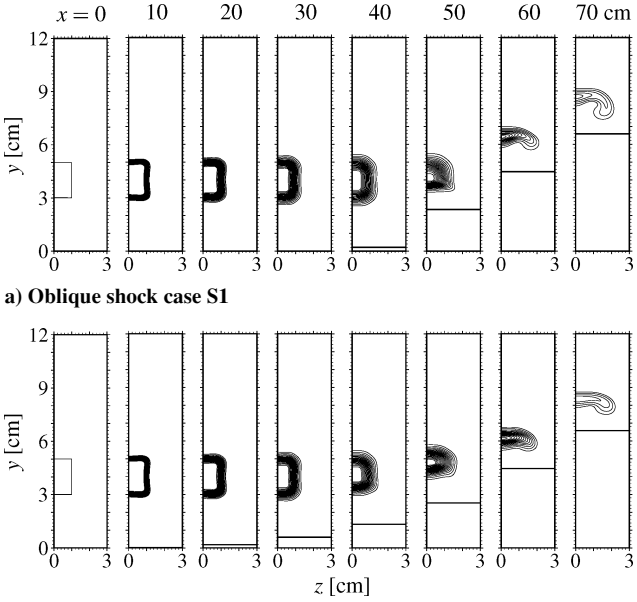

a) Oblique shock case S1

b) Compression fan case F1

Fig. 9 Comparison of the hydrogen mass fraction contours between cases a) S1 and b) F1 for the mixing enhancement by compression study; the contours of the mass fraction of hydrogen are fixed to $c_{H_2} = 0.05,\ 0.10, \ldots, 0.90,\ 0.95$.

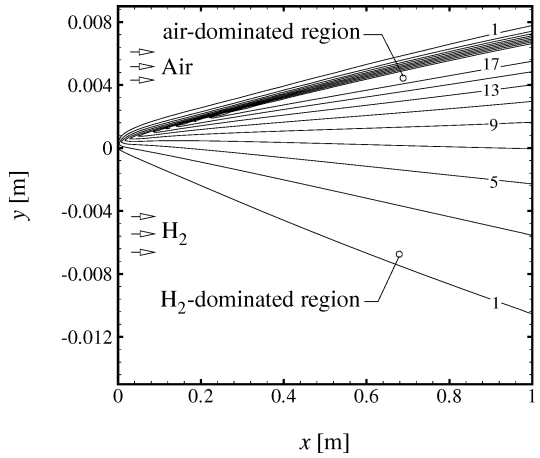

Fig. 10 Contours of the mass flow of reacting oxygen, $\rho u c^R_{O_2}$, in kg/m^{2}s for a hydrogen/air planar mixing layer with inflow conditions set to state 1.

The reason that the mixing efficiency growth of a hydrogen–air mixing layer is mostly dependent on the growth of the mixing layer in the air-dominated region can be seen through the definition of the mixing efficiency, which, at a given x station, is recalled to correspond to

$$\eta_m \propto \iint \rho u c^R_{O_2}\, dy\, dz$$

Taking, for example, a hydrogen/air mixing layer occurring in state 1, it is seen that the contribution to the mixing efficiency by the flow in the hydrogen-dominated region of the mixing layer is small due to 1) the product between the density and the streamwise velocity of the hydrogen stream being approximately 4.7 times less than the one of the air stream, and 2) the reacting mass fraction of oxygen $c^R_{O_2}$ reaching a maximum when the mass fraction of hydrogen is 0.02876, which occurs in the air-dominated region near the edge of the mixing layer. Therefore, for a hydrogen–air mixing layer occurring in state 1, most of the mass flux of reacting oxygen is situated near the edge of the mixing layer in the oxygen-dominated region, which is the reason that the mixing efficiency growth is not affected significantly by a change in mixing layer growth in the hydrogen-dominated region. This is confirmed by the contours of $\rho u c^R_{O_2}$ shown in Fig. 10 for a planar mixing layer problem with the inflow conditions of air and hydrogen set to those in state 1. Most of the mass flow of reacting oxygen can be seen to be situated in the air-dominated region, with a significantly lesser amount being present in the hydrogen-dominated region.

Range of Applicability of the Mixing Efficiency Growth Equation

It is emphasized that the quantitative assessment of the sole effect of interface stretching due to the axial vortices induced by an oblique shock or a compression fan is based on the mixing efficiency growth equation outlined in Eq. (8). The derivation of Eq. (8) involved two major assumptions:

1) The speeds of the hydrogen and air streams are not altered through the compression process, and

2) The density ratios for the fuel and air streams are identical between the states upstream and downstream of the compression process.

The assumption of the same density ratio increase for the air and the hydrogen is found to be exactly correct if both the hydrogen and air streams are subject to the same pressure increase ratio and if the type of compression process for both streams is the same (either isentropic compression or oblique shock compression). Because it is likely that both streams are subject to the same type of compression process, and since the effective pressure variations in the postcompression mixing layer are observed numerically not to vary by more than 20% from the mean, it hence follows that the assumption of identical density ratio increase for the air and hydrogen streams is a fairly good one. This is confirmed by probing the hydrogen and air properties for case F1 at stations $x = 10$ cm and $x = 50$ cm: for the same pressure increase, the density ratio of hydrogen is found to be within 1% of the density ratio of air. It is noted that the error associated with variations in the pressure is expected to create only local changes in the mixing efficiency growth, which are here filtered by taking an average mixing efficiency growth over a relatively long streamwise distance.

However, it is not quite as clear whether the assumption of unaltered hydrogen and air speeds is valid. As stated by Swithenbank et al.,[3] the speed of the flow in a hypersonic engine cannot be altered significantly, due to 1) the total energy of the incoming air being almost entirely kinetic and 2) the restriction of a maximum cycle temperature in the engine. The latter condition effectively prevents a significant portion of the kinetic energy from being transformed into thermal energy, hence resulting in a quasi-constant air speed through the engine. It follows that the assumption of a constant speed for the air stream through the compression process is adequate in this case, which is confirmed by the small 5% deviation observed numerically for either case S1 or F1. On the other hand, the inflow Mach number of the hydrogen is considerably less than the inflow Mach number of the air (Mach 4.44 vs Mach 7.74), which makes the hydrogen stream subject to a more significant flow deceleration for the same pressure increase ratio. This is confirmed numerically, as a decrease in the hydrogen flow speed by approximately 2–3% is observed for the compression fan case F1 from $x = 10$ cm to $x = 50$ cm, whereas the air flow speed is seen to vary by only 1% over the same distance. Unfortunately, it is not possible to measure the hydrogen flow speed throughout the compression process due to the jet being eroded by the boundary layer beyond $x = 50$ cm. Nonetheless, assuming that the hydrogen speed would continue to decrease at the same rate downstream from $x = 50$ cm, it can be approximated to be 10–15% less than its original speed.

It is recalled that a change in hydrogen speed influences the growth of the mixing layer through the incompressible average vortex speed and through the speed difference between the two streams, as outlined in Eq. (6). Because the hydrogen stream density is considerably less than the air density, the incompressible average vortex speed can be taken as being equal to the air speed, which, as mentioned earlier, can be assumed to be constant through the compression process. Therefore, it is seen that the assumption in Eq. (8) of a constant incompressible average vortex speed through the compression process is an excellent one. However, a 10% reduction in the hydrogen stream speed due to compression reduces the speed difference between the two streams (hence, the-shear in the mixing layer) by approximately 25%. Therefore, we note that the calculated amount of interface stretching due to axial vortices is probably underestimated by 25%, due to Eq. (8) not taking into account the shear loss through the compression process due to the reduced hydrogen stream speed.

Although a fairly good assumption for the compression fan and oblique shock problems shown herein (with an associated error of approximately 25%), the assumption of unaltered hydrogen and air speeds cannot be made for any type of hypersonic hydrogen/air mixing configuration, and special care must be taken in applying Eq. (8) to a different problem. The use of Eq. (8) is expected to induce substantial error when either 1) the Mach number of the hydrogen stream is not sufficiently high or 2) the air and hydrogen speeds are closely matched prior to the compression process.

Another source of error in the application of Eq. (8) is the discrepancy between the Papamoschou–Roshko correction term and the $k\omega$ turbulence model in the convective Mach number range $0.8 \leq M_c \leq 1.2$. It is probable that this error is more important in case S1 than in case F1, since the change in convective Mach number through the oblique shock is greater than the change in convective Mach number through the compression fan. It hence follows that the

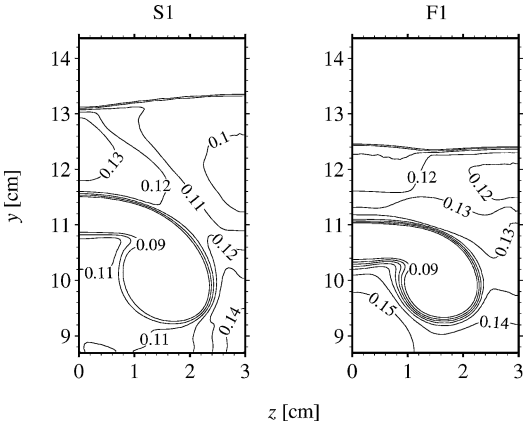

Fig. 11 Comparison of the density contours (kg/m^3) between cases S1 and F1 at $x = 80$ cm.

interface length stretching due to axial vortices is underpredicted because of this discrepancy between the Papamoschou–Roshko correction term and the $k\omega$ turbulence model and that the underprediction is probably more pronounced for the oblique shock case than for the compression fan case. This provides a possible explanation to the fact that the interface length obtained numerically (as shown through the hydrogen mass fraction contours in Fig. 9 and the density contours in Fig. 11) is seen to be approximately 20% higher for the oblique shock case than for the compression fan case, whereas the interface length stretching due to axial vortices [as predicted by Eq. (8)] shows an increase of only 3%.

Finally, it should be mentioned that in addition to the assumptions already stated, Eq. (8) makes the implicit assumption that the only shear present is due to the speed difference between hydrogen and air. Axial vortices induce a substantial amount of cross-stream shear, which contributes to the spread of the mixing layer at a low convective Mach number.[16] At a high convective Mach number, such as the one in use in this paper, the impact of the cross-stream shear on the mixing efficiency is minimized.[16] Therefore, the convective Mach number must be high for Eq. (8) to predict the mixing efficiency growth accurately, due to the high impact of cross-stream shear on the mixing layer growth at a low convective Mach number.

Conclusions

Based on the available empirical correlations for a free turbulent shear layer, an expression (dubbed the "mixing efficiency growth equation") is derived to predict the mixing efficiency increase through a compression wave for the special case of a high-convective-Mach-number mixing layer in which both streams are at a high Mach number. In such conditions, it is seen that two assumptions can be made: 1) the speed of the fuel and air streams can be taken as constant through the compression and 2) the density increase of the fuel can be taken equal to the density increase of the air through the compression. From these two assumptions, it is then shown that the mixing efficiency growth is proportional to the product of the flow density, the interface length, and the Papamoschou–Roshko correction term. Noting that the Papamoschou–Roshko correction term decreases for decreasing temperature, this shows one of the major challenges of mixing in a shcramjet inlet. The very low flow density and flow temperature lead to very low mixing efficiency growth in a shcramjet inlet, as compared to the mixing efficiency growth that could be obtained in a scramjet combustor, where the temperature and the density are high.

The numerical results obtained show that the mixing efficiency growth increases through an oblique shock and a Prandtl–Meyer compression fan are of 5.7 and 6.3 times, respectively. With the help of the derived mixing efficiency growth equation, it is deduced that the greater mixing efficiency growth increase through the compression fan is a consequence of the higher density induced by the compression fan, despite the more vigorous interface stretching by the axial vortices induced by the oblique shock.

Acknowledgments

This work has been supported by the Natural Sciences and Engineering Research Council (NSERC). The first author thanks all writers of free software for donating the compilers, typesetting software, and vector-drawing programs that were used.

References

[1]Sislian, J. P., and Atamanchuk, T. M., "Aerodynamic and Propulsive Performance of Hypersonic Detonation Wave Ramjets," *Proceedings of the 9th International Symposium on Air-Breathing Engines*, edited by F. Billig, AIAA, Washington, DC, 1989, pp. 1026–1035.

[2]Sislian, J. P., "Detonation Wave Ramjets," *Scramjet Propulsion*, edited by E. T. Curran and S. N. B. Murthy, Vol. 189, Progress in Aeronautics and Astronautics, AIAA, Reston, VA, 2001, Chap. 13, pp. 823–889.

[3]Swithenbank, J., Eames, I. W., Chin, S. B., Ewan, B. C. R., Yang, Z., Cao, J., and Zhao, X., "Turbulent Mixing in Supersonic Combustion Systems," *High-Speed Flight Propulsion Systems*, edited by S. N. B. Murthy and E. T. Curran, Vol. 137, Progress in Aeronautics and Astronautics, AIAA, Washington, DC, 1991, Chap. 6, pp. 341–383.

[4]Marble, F., Zukoski, E., Jacobs, J., Hendricks, G., and Waitz, I., "Shock Enhancement and Control of Hypersonic Mixing and Combustion," AIAA Paper 90-1981, 1990.

[5]Vasilev, V. I., Zokotenko, S. N., Krasheninnikov, S. J., and Stepanov, V. A., "Numerical Investigation of Mixing Augmentation Behind Oblique Shock Waves," *AIAA Journal*, Vol. 32, No. 2, 1994, pp. 311–316.

[6]Lee, S.-H., Jeung, I.-S., and Yoon, Y., "Computational Investigation of Shock-Enhanced Mixing and Combustion," *AIAA Journal*, Vol. 35, No. 12, 1997, pp. 1813–1820.

[7]Nedungadi, A., and Lewis, M. J., "Numerical Study of Fuel Mixing Enhancement Using an Oblique Shock/Vortex Interaction," *Journal of Propulsion and Power*, Vol. 16, No. 6, 2000, pp. 946–955.

[8]Waitz, I. A., Qiu, Y. J., Manning, T. A., Fung, A. K. S., Elliot, J. K., Kerwin, J. M., Krasnodebski, J. K., O'Sullivan, M. N., Tew, D. E., Greitzer, E. M., Marble, F. E., Tan, C. S., and Tilman, T. G., "Enhanced Mixing with Streamwise Vorticity," *Progress in Aerospace Science*, Vol. 33, 1997, pp. 323–351.

[9]Waitz, I., Marble, F., and Zukoski, E., "An Investigation of a Contoured Wall Injector for Hypervelocity Mixing Augmentation," AIAA Paper 91-2265, 1991.

[10]Waitz, I., Marble, F., and Zukoski, E., "Vorticity Generation by Contoured Wall Injectors," AIAA Paper 92-3550, 1992.

[11]Waitz, I., Marble, F., and Zukoski, E., "A Systematic Experimental and Computational Investigation of a Class of Contoured Wall Fuel Injectors," AIAA Paper 92-0625, 1992.

[12]Waitz, I. A., Marble, F. E., and Zukoski, E. E., "Investigation of a Contoured Wall Injector for Hypervelocity Mixing Augmentation," *AIAA Journal*, Vol. 31, No. 6, 1993, pp. 1014–1021.

[13]Lee, S.-H., Jeung, I.-S., and Yoon, Y., "Computational Investigation of Shock-Enhanced Mixing: Application to Circular Cross Section Combustor," *AIAA Journal*, Vol. 36, No. 11, 1998, pp. 2055–2062.

[14]Shau, Y. R., and Dolling, D. S., "Experimental Study of Spreading Rate Enhancement of High Mach Number Turbulent Shear Layers," AIAA Paper 89-2458, 1989.

[15]Parent, B., and Sislian, J. P., "The Use of Domain Decomposition in Accelerating the Convergence of Quasihyperbolic Systems," *Journal of Computational Physics*, Vol. 179, No. 1, 2002, pp. 140–169.

[16]Parent, B., Sislian, J. P., and Schumacher, J., "Numerical Investigation of the Turbulent Mixing Performance of a Cantilevered Ramp Injector," *AIAA Journal*, Vol. 40, No. 8, 2002, pp. 1559–1566.

[17]Wilcox, D. C., "Reassessment of the Scale Determining Equation for Advanced Turbulence Models," *AIAA Journal*, Vol. 26, No. 11, 1988, pp. 1299–1310.

[18]Yee, H. C., Klopfer, G. H., and Montagné, J.-L., "High-Resolution Shock-Capturing Schemes for Inviscid and Viscous Hypersonic Flows," *Journal of Computational Physics*, Vol. 88, 1990, pp. 31–61.

[19]Wilcox, D. C., "Dilatation–Dissipation Corrections for Advanced Turbulence Models," *AIAA Journal*, Vol. 30, No. 11, 1992, pp. 2639–2646.

[20]Dimotakis, P. E., "Turbulent Mixing and Combustion," *High-Speed Flight Propulsion Systems*, edited by S. N. B. Murthy and E. T. Curran, Vol. 137, Progress in Aeronautics and Astronautics, AIAA, Washington, DC, 1991, Chap. 5, pp. 265–340.
[21]Brown, G. L., "The Entrainment and Large Structure in Turbulent Mixing Layers," *Proceedings of the 5th Australasian Conference on Hydraulics and Fluid Mechanics*, edited by D. Lindley and A. Y. Sutherland, Univ. of Canterbury, Christchurch, New Zealand, 1974, pp. 352–359.
[22]Brown, G. L., and Roshko, A., "On Density Effects and Large Structure in Turbulent Mixing Layers," *Journal of Fluid Mechanics*, Vol. 64, 1974, pp. 775–781.
[23]Papamoschou, D., and Roshko, A., "The Compressible Turbulent Shear Layer: An Experimental Study," *Journal of Fluid Mechanics*, Vol. 197, 1988, pp. 453–477.
[24]Parent, B., and Sislian, J. P., "Turbulent Hypervelocity Fuel/Air Mixing by Cantilevered Ramp Injectors," AIAA Paper 2001-1888, April 2001.
[25]Parent, B., "Computational Study of Fuel Injection in a Shcramjet Inlet," Ph.D. Dissertation, Graduate Dept. of Aerospace Science and Engineering, Univ. of Toronto, Toronto, Aug. 2002.

G. M. Faeth
Former Editor-in-Chief